

## Fractional-order Maxwell model of seabed mud and its effect on surface-wave damping\*

Yue-zhang XIA (夏乐章), Ke-qin ZHU (朱克勤)

(Department of Engineering Mechanics, Tsinghua University, Beijing 100084, P. R. China)

**Abstract** A fractional-order Maxwell model is used to describe the viscoelastic seabed mud. The experimental data of the real mud well fit the results of the fractional-order Maxwell model that has fewer parameters than the traditional model. The model is then used to investigate the effect of the mud on the surface-wave damping. The damping rate of a linear monochromatic wave is obtained. The elastic resonance of the mud layer is observed, which leads to the peaks in the damping rate. The damping rate is a sum of the modal damping rates, which indicates the wave damping induced by the mud motion of particular modes. The analysis shows that near the resonance, the total damping rate is dominated by the damping rate of the corresponding mode.

**Key words** seabed mud, wave-mud interaction, wave damping, fractional-order Maxwell model

**Chinese Library Classification** O353.2

**2010 Mathematics Subject Classification** 76A05, 76B15

### 1 Introduction

In coastal areas, the existence of a muddy seabed can significantly dissipate the energy of the free-surface water waves<sup>[1]</sup>. Since the mud rheology varies with sites and environments, various types of mud models have been proposed, among which the viscoelastic models are common<sup>[2]</sup>. These traditional linear viscoelastic models can be covered by a generalized viscoelastic model<sup>[3]</sup>.

The traditional viscoelastic models have some defects in mud modeling. Jiang and Mehta<sup>[4]</sup> used a Kevin-Voigt model to fit their experimental data. However, their parameters of the model vary with the wave frequency. Krotov<sup>[3]</sup> expressed the results of Jiang and Mehta<sup>[4]</sup> in the form of complex viscosities and fitted them with a generalized viscoelastic model. However, his model has eight parameters, and the resulting constitutive equation has high-order derivatives, which may increase the difficulty in the analysis of wave-mud interactions.

Compared with the traditional viscoelastic models, the fractional-order models provide a higher level of adequacy<sup>[5]</sup> and may overcome the above defects. In the rheology of polymers, a fractional-order Maxwell model is used, which relates with the stress tensor  $\tau'$  and the strain tensor  $\epsilon$  by<sup>[5]</sup>

$$\tau' + B' \frac{\partial^{(\theta_1-\theta_2)} \tau'}{\partial t'^{(\theta_1-\theta_2)}} = A' \frac{\partial^{\theta_1} \epsilon}{\partial t'^{\theta_1}}, \quad 0 \leq \theta_1, \theta_2 \leq 1, \quad (1)$$

\* Received Apr. 11, 2011 / Revised Aug. 24, 2011

Project supported by the National Natural Science Foundation of China (No. 10972117)

Corresponding author Yue-zhang XIA, Ph. D., E-mail: jlz02@mails.tsinghua.edu.cn

in which the fractional derivative  $\frac{\partial^\theta}{\partial t^\theta}$  is defined as<sup>[5]</sup>

$$\frac{\partial^\theta}{\partial t^\theta} f(t) = \frac{\partial^{(\theta-1)}}{\partial t^{(\theta-1)}} \dot{f}(t) = \frac{1}{\Gamma(1-\theta)} \int_0^t (t-t^*)^{-\theta} \dot{f}(t^*) dt^*, \quad 0 < \theta < 1. \quad (2)$$

If the material is under the harmonic motion with the circular frequency  $\omega'$ , (1) yields

$$\tau' = \mu'(\omega') \frac{\partial \epsilon}{\partial t'}, \quad \mu'(\omega') = \frac{A'(-i\omega')^{\theta_1-1}}{1 + B'(-i\omega')^{\theta_1-\theta_2}} = |\mu'(\omega')| e^{i\theta'(\omega')}. \quad (3)$$

The complex viscosity  $\mu'(\omega')$  in (3) can then be used to fit the mud data of Jiang and Mehta<sup>[4]</sup>. Choosing the parameters in Table 1 yields that the fitting is quite good, as illustrated in Fig. 1. Compared with the Kelvin-Voigt model<sup>[4]</sup>, the parameters of the fractional-order Maxwell model are fixed. In comparison with Krotov's eight-parameter model with derivatives up to fourth order<sup>[3]</sup>, the fractional-order Maxwell model has fewer parameters, and the high-order derivatives are avoided.

Since the fractional-order Maxwell model has some benefits in mud rheology, we use this model to investigate the interaction between the mud and the sinusoidal waves.

**Table 1** Parameters of fractional-order Maxwell model defined by (1)

Mud type	$\theta_1$	$\theta_2$	$B'$	$A'$
KI*, $\phi = 0.12$	0.040	0.585	0.300	$1.55 \times 10^4$
OK*, $\phi = 0.11$	0.060	0.450	0.450	$6.00 \times 10^2$
MB*, $\phi = 0.07$	0.030	0.380	0.600	$1.35 \times 10^2$
MB*, $\phi = 0.11$	0.015	0.295	0.450	$1.50 \times 10^3$
MB*, $\phi = 0.17$	0.025	0.375	0.450	$9.50 \times 10^3$
AK*, $\phi = 0.12$	0.020	0.586	0.410	$7.00 \times 10^3$

\*KI: Kerala, India mud, OK: Okeechobee mud, MB: Mobile Bay mud, and AK: mud mainly composed of attapulgite and kaolinite

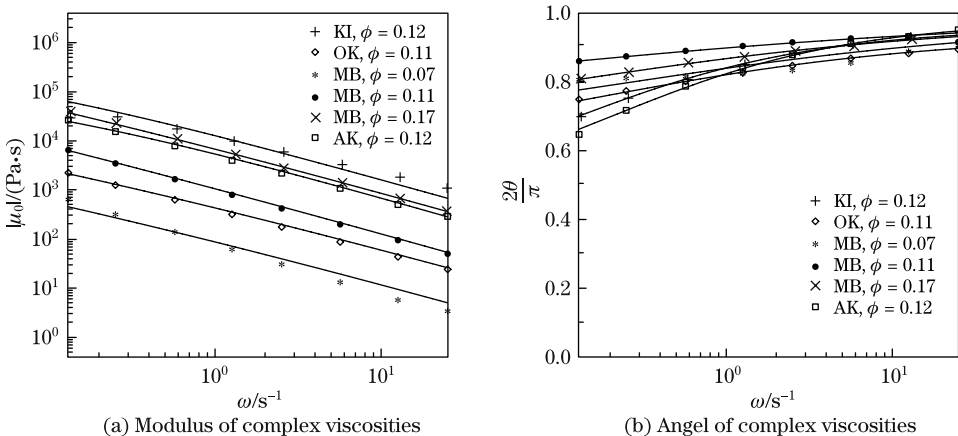


**Fig. 1** Fitting of complex viscosities of fractional-order Maxwell model (solid lines) to complex viscosities calculated from mud data of Jiang and Mehta<sup>[4]</sup> (separated points), where the mud data are obtained under monochromatic wave with circular frequencies  $\omega = 0.13, 0.25, 0.57, 1.26, 2.51, 5.65, 12.6, 25.1$  rad/s

## 2 Mathematical formulation

The physical problem of the wave-mud interaction is investigated in a two-layered water-mud system, as illustrated in Fig. 2. The Cartesian coordinates are set on the surface of the still water with the  $x'$ -axis pointing to the right and the  $z'$ -axis pointing upwards. The thickness of the water layer and the thickness of the mud layer are  $h'$  and  $d'$ , respectively. The wave height is  $a'_0$ , and the wave length is  $l'_0$ . The free surface displacement  $\zeta'$  is a function of the horizontal coordinate  $x'$  and the time  $t'$ . The water density and the mud density are  $\rho'_w$  and  $\rho'_m$ , respectively. The water is assumed to be inviscid. Furthermore, the water motion is assumed to be irrotational, and the interfacial mixing is ignored. The viscoelastic mud is described by the fractional-order Maxwell model defined by (1), whose complex viscosity under the sinusoidal waves is given by (3). The primes are used to distinguish all the dimensional variables from their dimensionless counterparts.

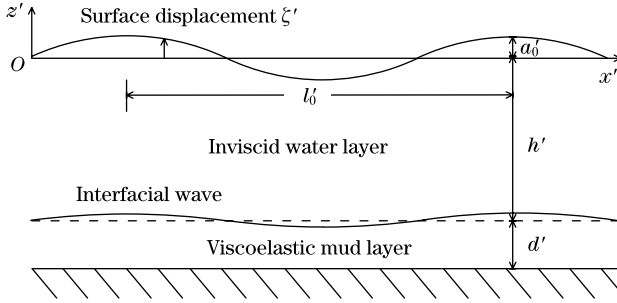


**Fig. 2** Sketch of two-layered water-mud system

In the water layer, the nondimensionalization takes the form

$$\begin{cases} x = \frac{x'}{l'_0}, \quad z = \frac{z'}{h'}, \quad \zeta = \frac{\zeta'}{a'_0}, \quad t = \frac{t'\sqrt{gh'}}{l'_0}, \\ u = \frac{u'_w}{\varepsilon\sqrt{gh'}}, \quad w_w = \frac{\mu w'_w}{\varepsilon\sqrt{gh'}}, \quad p_w = \frac{p'_w}{\rho'_w g a'_0}, \\ \mu = \frac{h'}{l'_0}, \quad \varepsilon = \frac{a'_0}{h'}, \end{cases} \quad (4)$$

where  $u_w$  and  $w_w$  are the dimensionless water velocities in the horizontal direction and the vertical direction, respectively. The variable  $p_w$  is the dimensionless dynamic pressure of the water. The two dimensionless numbers  $\mu$  and  $\varepsilon$  denote the strength of the frequency dispersion and the nonlinear effect, respectively.

In the mud layer, the nondimensionalization takes the form

$$\begin{cases} \eta = \frac{\mu(z' + h')}{\alpha h'}, \quad d = \frac{d'}{\alpha l'_0}, \quad \tau_{m,xz} = \frac{\tau'_{m,xz}}{\alpha \rho'_m g a'_0}, \\ u_m = \frac{u'_m}{\varepsilon\sqrt{gh'}}, \quad w_m = \frac{w'_m}{\alpha\varepsilon\sqrt{gh'}}, \quad p_m = \frac{p'_m}{\rho'_m g a'_0}, \\ \alpha^2 = \frac{A' \left( \frac{\sqrt{gh'}}{l'_0} \right)^{\theta_1 - 1}}{\rho'_m l'_0 \sqrt{gh'}}, \quad \lambda = B' \left( \frac{\sqrt{gh'}}{l'_0} \right)^{\theta_1 - \theta_2}, \quad \gamma = \frac{\rho'_w}{\rho'_m}, \end{cases} \quad (5)$$

where  $\eta$  is a new vertical coordinate within the mud layer, and  $\tau_{m,xz}$  is a component of the dimensionless mud stress tensor. The variables  $u_m$  and  $w_m$  denote the dimensionless mud velocities on the horizontal direction and the vertical direction, respectively.  $\alpha$ ,  $\lambda$ ,  $\theta_1$ , and  $\theta_2$  are the dimensionless parameters of the fractional-order Maxwell model. Since  $A'_m(\sqrt{gh'}/l'_0)^{\theta_1-1}$  has a dimension of the dynamic viscosity, the dimensionless number  $\alpha^2$  is similar to the inverse of the Reynolds number.

As compared with the traditional Maxwell model, a similar assumption to that of Xia and Zhu<sup>[6]</sup> is required as follows:

$$O(\alpha) \sim O(\varepsilon^2) \sim O(\mu^4), \quad d \sim O(1), \quad (6)$$

where the assumption  $O(\varepsilon) \sim O(\mu^2)$  is the Boussinesq approximation, and the assumption  $O(\alpha) \sim O(\varepsilon^2)$  indicates that the influence of the viscous mud is weak, as compared with the wave nonlinearity. The perturbation analysis then leads to a set of Boussinesq equations<sup>[6-7]</sup> as follows:

$$\frac{1}{\varepsilon} \frac{\partial H}{\partial t} + \frac{\partial}{\partial x}(H\bar{u}) = \frac{\alpha}{\mu} w_{mi} + O(\mu^4), \quad (7)$$

$$\frac{\partial \bar{u}}{\partial t} + \varepsilon \bar{u} \frac{\partial \bar{u}}{\partial x} + \frac{1}{\varepsilon} \frac{\partial H}{\partial x} - \frac{\mu^2}{3} \frac{\partial^2}{\partial x^2} \frac{\partial \bar{u}}{\partial t} = O(\mu^4), \quad (8)$$

where  $H(x, t) \equiv 1 + \varepsilon \zeta(x, t)$  is the transient water layer thickness. The depth-averaged horizontal velocity of the water layer  $\bar{u}(x, t)$  is defined as

$$\bar{u} \equiv \frac{1}{H} \int_{-1}^{\varepsilon \zeta} u_w dz = u_b - \frac{\mu^2}{6} H^2 \frac{\partial^2 u_b}{\partial x^2} + O(\mu^4), \quad (9)$$

where  $u_b$  is the horizontal water velocity on the water-mud interface. The source term  $w_{mi}$  appearing in the continuity equation (7) is the vertical mud velocity on the water-mud interface.

For the linear waves,  $\varepsilon$  tends to zero, and the linearized (7) and (8) can yield

$$\left(1 - \frac{\mu^2}{3} \frac{\partial^2}{\partial x^2}\right) \frac{\partial^2 \zeta}{\partial t^2} - \frac{\partial^2 \zeta}{\partial x^2} = \frac{\alpha}{\mu} \frac{\partial w_{mi}}{\partial t} + O(\mu^4), \quad (10)$$

in which the influence of the mud layer is  $O(\alpha/\mu)$ . This term should be solved from the mud dynamics equation. The leading-order equations of the mud layer are

$$\frac{\partial u_m}{\partial x} + \frac{\partial w_m}{\partial \eta} = 0, \quad -d \leq \eta \leq 0, \quad (11)$$

$$\gamma \frac{\partial u_b}{\partial t} + \frac{\partial \tau_{m,xz}}{\partial \eta} = \frac{\partial u_m}{\partial t}, \quad -d \leq \eta \leq 0, \quad (12)$$

$$\tau_{m,xz} + \lambda \frac{\partial^{(\theta_1-\theta_2)} \tau_{m,xz}}{\partial t^{(\theta_1-\theta_2)}} = \frac{\partial^{(\theta_1-1)}}{\partial t^{(\theta_1-1)}} \frac{\partial u_m}{\partial \eta}, \quad -d \leq \eta \leq 0. \quad (13)$$

The boundary conditions are

$$u_m = 0, \quad w_m = 0 \quad \text{at} \quad \eta = -d, \quad (14)$$

and the matching conditions are

$$w_{mi} \equiv w_m, \quad \tau_{m,xz} = 0 \quad \text{at} \quad \eta = 0. \quad (15)$$

Substituting (8), (9), and (13) into (12) yields

$$\frac{\partial u_m}{\partial t} = -\gamma \frac{\partial \zeta}{\partial x} + L_{\partial t} \frac{\partial^2 u_m}{\partial \eta^2}, \quad -d \leq \eta \leq 0, \quad (16)$$

where the linear operator  $L_{\partial t}$  is defined as

$$L_{\partial t} = \frac{\frac{\partial^{(\theta_1-1)}}{\partial t^{(\theta_1-1)}}}{1 + \frac{\lambda \partial^{(\theta_1-\theta_2)}}{\partial t^{(\theta_1-\theta_2)}}}. \quad (17)$$

By the boundary conditions (14) and the interfacial conditions (15), the horizontal velocity  $u_m$  can be expressed by the Fourier expanding as follows:

$$u_m(x, \eta, t) = \frac{2}{d} \sum_{n=1}^{\infty} (-1)^{n-1} \frac{\cos(b_n \eta)}{b_n} u_{m,n}(x, t), \quad b_n = \frac{(n - \frac{1}{2})\pi}{d}, \quad (18)$$

where  $\cos(b_n \eta)$  indicates the velocity profile of the  $n$ th mode. Substituting (18) into (16) yields

$$\left( \frac{\partial}{\partial t} + b_n^2 L_{\partial t} \right) u_{m,n} = -\gamma \frac{\partial \zeta}{\partial x}. \quad (19)$$

According to (11), the vertical velocity  $w_{mi}$  can be integrated from the mud bottom as

$$w_{mi} = -\frac{2}{d} \sum_{n=1}^{\infty} \frac{1}{b_n^2} \frac{\partial u_{m,n}}{\partial x}. \quad (20)$$

Introduce a moving coordinate  $\sigma$  and a slow-varying time-scale  $\xi$  by

$$\sigma = t - (x - x_0), \quad \xi = \frac{\alpha}{\mu} t. \quad (21)$$

Then, (10) becomes

$$2 \frac{\alpha}{\mu} \frac{\partial \zeta}{\partial \xi} - \frac{\mu^2}{3} \frac{\partial^3 \zeta}{\partial \sigma^3} = \frac{\alpha}{\mu} w_{mi} + O(\mu^4), \quad (22)$$

in which the term “ $-\mu^2 \frac{\partial^3 \zeta}{3 \partial \sigma^3}$ ” denotes the dispersion induced by the water layer thickness. The leading-order equations (19) and (20) for  $w_{mi}$  become

$$\begin{cases} w_{mi} = \frac{2}{d} \sum_{n=1}^{\infty} \frac{1}{b_n^2} \frac{\partial u_{m,n}}{\partial \sigma}, \\ \left( \frac{\partial}{\partial \sigma} + b_n^2 L_{\partial \sigma} \right) u_{m,n} = \gamma \frac{\partial \zeta}{\partial \sigma}. \end{cases} \quad (23)$$

For the linear progressive waves, the variables can be represented in the form of

$$(\zeta(\sigma, \xi), w_{mi}(\sigma, \xi), u_{m,n}(\sigma, \xi)) = (\tilde{\zeta}(\xi), \tilde{w}_{mi}(\xi), \tilde{u}_{m,n}(\xi)) e^{i\sigma}. \quad (24)$$

Substituting (24) into (23) yields

$$\tilde{w}_{mi} = \tilde{\zeta} \frac{2\gamma}{d} \sum_{n=1}^{\infty} \frac{i}{b_n^2} \frac{1 + \lambda i^{\theta_1 - \theta_2}}{1 - b_n^2 i^{\theta_1} + \lambda i^{\theta_1 - \theta_2}}. \quad (25)$$

Substituting (24) and (25) into (22) yields

$$\frac{d\tilde{\zeta}(\xi)}{d\xi} = i \left( \frac{\mu^3}{6\alpha} + \frac{\gamma}{d} \sum_{n=1}^{\infty} \frac{1}{b_n^2} \frac{1 + \lambda i^{\theta_1 - \theta_2}}{1 - b_n^2 i^{\theta_1} + \lambda i^{\theta_1 - \theta_2}} \right) \tilde{\zeta}(\xi). \quad (26)$$

We can express  $\tilde{\zeta}(\xi)$  in the following form:

$$\tilde{\zeta}(\xi) = a_0 e^{i\beta\xi}, \quad \beta = \frac{\mu^3}{6\alpha} + \beta_r + i\beta_i, \quad (27)$$

where the term “ $\mu^3/(6\alpha)$ ” is the dispersion rate of the water layer.  $\beta_r$  and  $\beta_i$  denote the dispersion rate and the damping rate of the mud layer, respectively. Substituting (27) into (26) yields

$$\beta_r = \frac{\gamma}{d} \sum_{n=1}^{\infty} \frac{1}{b_n^2} \operatorname{Re} \left( \frac{1 + \lambda i^{\theta_1 - \theta_2}}{1 - b_n^2 i^{\theta_1} + \lambda i^{\theta_1 - \theta_2}} \right), \quad (28)$$

$$\beta_i = \frac{\gamma}{d} \sum_{n=1}^{\infty} \frac{1}{b_n^2} \operatorname{Im} \left( \frac{1 + \lambda i^{\theta_1 - \theta_2}}{1 - b_n^2 i^{\theta_1} + \lambda i^{\theta_1 - \theta_2}} \right). \quad (29)$$

If  $\theta_1 = 1$  and  $\theta_2 = 0$ , the fractional-order Maxwell model degenerates into the traditional Maxwell model, and (29) becomes

$$\beta_i = \frac{\gamma}{d} \sum_{n=1}^{\infty} \frac{1}{b_n^4 - \lambda b_n^2 + \lambda^2 + 1}, \quad (30)$$

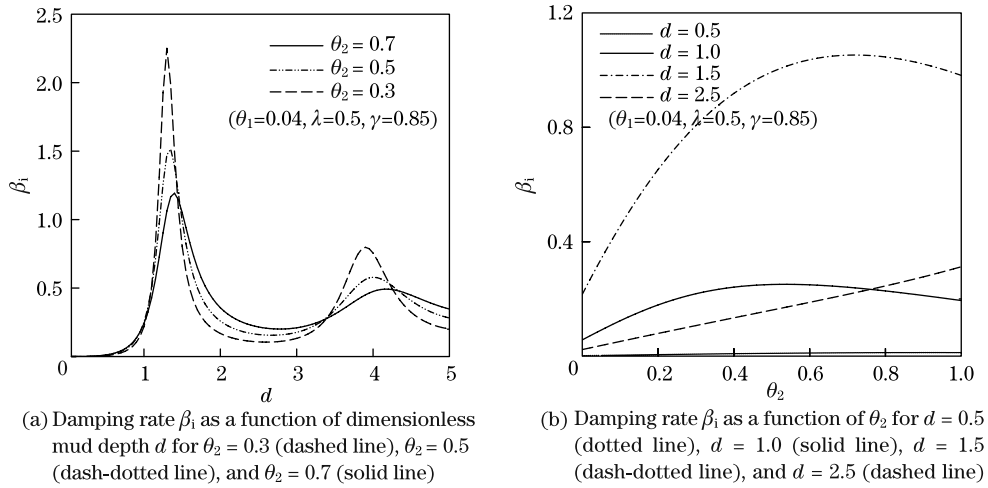
which agrees the equation 3.11 of Xia and Zhu<sup>[6]</sup>.

### 3 Results and discussion

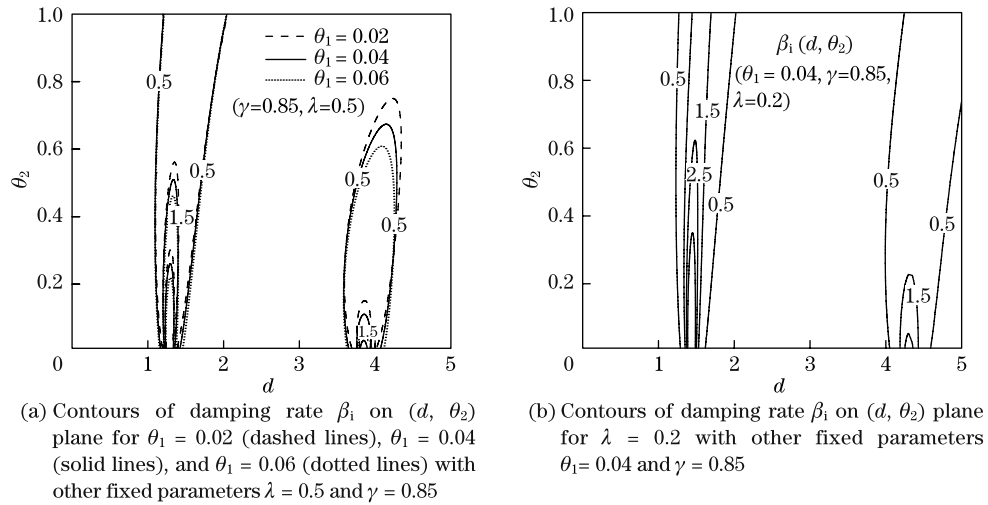
The damping rate  $\beta_i$  is a function of the dimensionless parameters  $\gamma$ ,  $d$ ,  $\lambda$ ,  $\theta_1$ , and  $\theta_2$ . In the following, we study the influence of the parameters  $d$  and  $\theta_2$  first and fix other parameters to simplify the analysis. We fix the density ratio  $\gamma$  to be 0.85, which is commonly used in [6–7]. We choose  $\theta_1$  to be 0.04, which is a moderate value in Table 1. In Fig. 1, the moderate wave frequency is  $O(1)$  Hz, and in Table 1, the parameter  $B'$  is around 0.5. Therefore, we fix the value of  $\lambda$  to be 0.5 according to (5).

Figure 3 illustrates the damping rate as a function of  $d$  or  $\theta_2$ . In Fig. 3(a), the curves of the damping rate always have peaks for any given  $\theta_2$ . The strong damping around  $d = 1.5$  indicates the existence of the elastic resonance. It is interesting that changing  $\theta_2$  does not significantly affect the position of the first peak, while the peak value does decrease with  $\theta_2$ . An explanation is that  $\theta_1$  is very small, which indicates the strong elasticity and determines the mud depth  $d$  of the resonance. Larger  $\theta_2$  indicates the stronger viscosity, which may weaken the mud motion near the resonance and lead to a smaller peak value of the damping rate. While far away from the resonance, the stronger viscosity (larger  $\theta_2$ ) strengthens the mud damping. The  $\beta_i$ - $\theta_2$  curves in Fig. 3(b) also indicate that for the mud depth far away from the resonance, the stronger viscosity leads to the stronger damping, since the damping rate  $\beta_i$  increases with  $\theta_2$  monotonously for  $d = 0.5$  and  $d = 2.5$ .

To consider the influence of the parameters  $\theta_1$  and  $\lambda$  on  $\beta_i$ , we illustrate the contours of  $\beta_i$  on the  $(d, \theta_2)$  plane in Fig. 4. According to Table 1, we know that  $\theta_1$  varies from 0.03 to 0.06. Figure 4(a) shows that changing  $\theta_1$  in this range does not significantly affect the structure of the contours. Since the wave frequency varies from 0.1 Hz to 20 Hz, the parameter  $\lambda$  will



**Fig. 3** Influence of parameters  $d$  and  $\theta_2$  on damping rate  $\beta_i$  with other fixed parameters  $\theta_1 = 0.04$ ,  $\lambda = 0.5$ , and  $\gamma = 0.85$



**Fig. 4** Sensitivity of damping rate  $\beta_i$  to parameters  $\theta_1$  and  $\lambda$

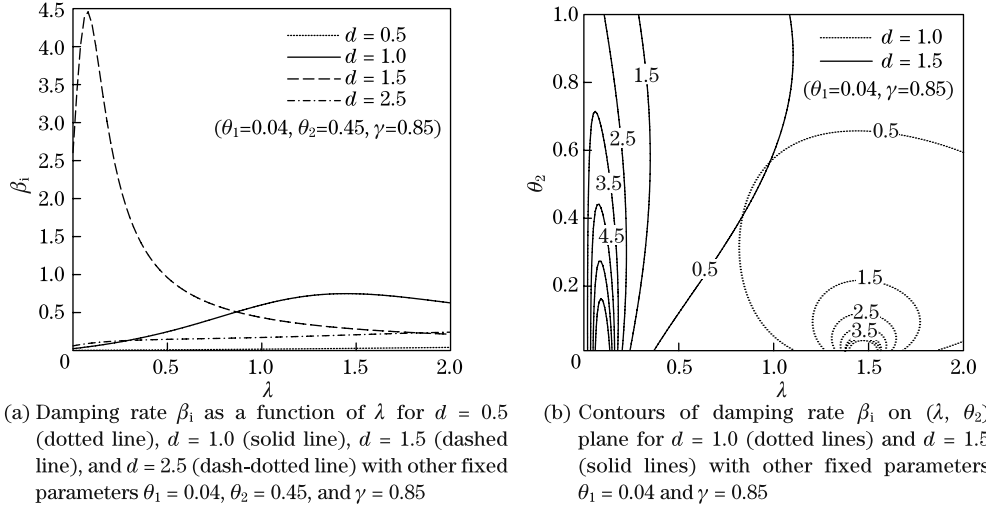
vary from 0.05 to 2, which significantly affect the damping rate, as shown in Fig. 4(b). The discussion for the influence is then discussed below.

Figure 5 shows the influence of the parameter  $\lambda$  on the damping rate  $\beta_i$ . In most cases,  $\beta_i$  varies with  $\lambda$  moderately, as illustrated in Fig. 5(a). Only for  $d = 1.5$ , an evident peak is observed, indicating the strong resonance. It is interesting that the corresponding value of  $\lambda$  is very small when the resonance occurs. According to (13),  $\lambda$  reflects the strength of the  $\theta_2$ -order derivative compared with the  $\theta_1$ -order derivative. Hence, small  $\lambda$  corresponds to the strong influence of the  $\theta_1$ -order derivative. According to Table 1,  $\theta_1$  is very close to 0. Thus, the fractional-order Maxwell model of small  $\lambda$  is very close to a elastic body, and that is why the strong resonance is observed. Figure 5(b) also indicates that for  $d = 1.0$ , which is far from the resonance depth, the damping rate  $\beta_i$  varies moderately in the parameter plane. When  $\beta_i$  reaches its peak, the corresponding  $\lambda$  is larger in the case of  $d = 1.0$ , as compared with the case of  $d = 1.5$ .

The modal analysis can be used to simplify the discussion. We can expand  $\beta_i$  into

$$\beta_i = \sum_{n=1}^{\infty} \beta_{in}, \quad \text{where} \quad \beta_{in} = \frac{\gamma}{db_n^2} \operatorname{Im} \left( \frac{1 + \lambda i^{\theta_1 - \theta_2}}{1 - b_n^2 i^{\theta_1} + \lambda i^{\theta_1 - \theta_2}} \right). \quad (31)$$

Then,  $\beta_{in}$  hereinafter is referred to as the modal damping rate. The modal damping rate  $\beta_{in}$  indicates the damping induced by the mud motion of the  $n$ th mode. Figure 6 illustrates the modal damping rates  $\beta_{in}$  as the functions of  $d$ . Similar to the results of the traditional Maxwell model<sup>[6]</sup>, each peak of the damping rate curve corresponds to the resonance of a particular mode. For  $d < 2.5$ , the mud damping is dominated by the motion of the first mode. Hence, for  $d < 2.5$ , we can use  $\beta_{i1}$  to study the property of the total damping rate  $\beta_i$ .



**Fig. 5** Influence of parameter  $\lambda$  on damping rate  $\beta_i$

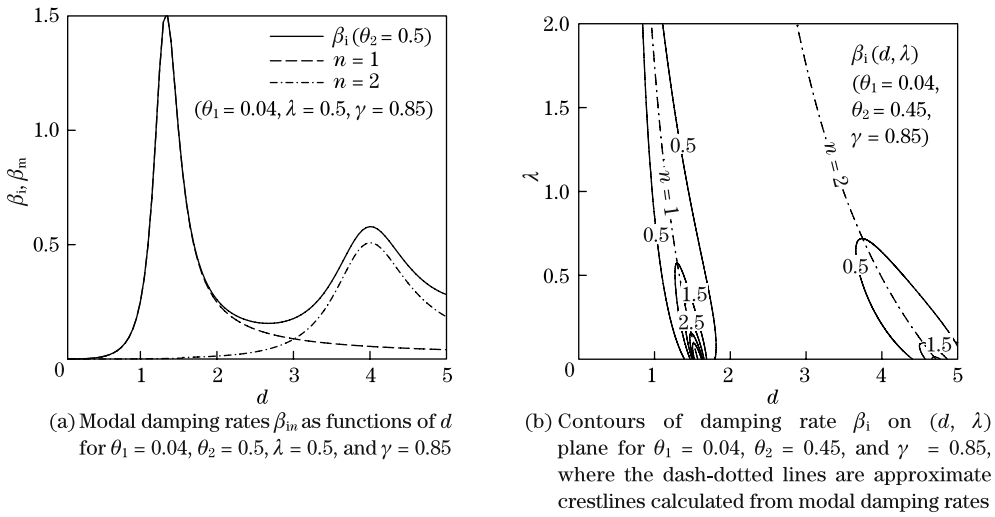


**Fig. 6** Contributions of modal damping rates  $\beta_{in}$  to total damping rates  $\beta_i$

According to (31), we have

$$\beta_{in} = \frac{\gamma}{d} \frac{\sin(\theta_1 \frac{\pi}{2}) + \lambda \sin(\theta_2 \frac{\pi}{2})}{1 + \lambda^2 + b_n^4 - 2b_n^2 \lambda \cos(\theta_2 \frac{\pi}{2}) - 2b_n^2 \cos(\theta_1 \frac{\pi}{2}) + 2\lambda \cos((\theta_1 - \theta_2) \frac{\pi}{2})}. \quad (32)$$

According to Table 1, where  $\theta_1 \approx 0$ , (32) is further simplified to

$$\beta_{in} = \frac{\gamma}{d} \frac{\lambda \sin(\theta_2 \frac{\pi}{2})}{1 + 2\lambda \cos(\theta_2 \frac{\pi}{2}) + \lambda^2 - 2(\lambda \cos(\theta_2 \frac{\pi}{2}) + 1)b_n^2 + b_n^4}. \quad (33)$$

According to (33), if  $\theta_1$  and  $\lambda$  are given,  $\beta_{in}$  reaches its peak at

$$\begin{aligned} b_{n,peak}^2 &= \frac{1}{3} \left( 1 + \lambda \cos(\theta_2 \frac{\pi}{2}) \right. \\ &\quad \left. + \sqrt{4 + 8\lambda \cos(\theta_2 \frac{\pi}{2}) + \lambda^2 (3 + \cos^2(\theta_2 \frac{\pi}{2}))} \right), \end{aligned} \quad (34)$$

which increases with  $\lambda$ . Since  $b_n$  is inversely proportional to  $d$  (see (18)), the resonance mud depth  $d_{peak}$  decreases with  $\lambda$ . That is why in Fig. 5(b), the contours move to the right (to larger  $\lambda$ ) when  $d$  changes from 1.5 to 1.0. According to (34), we can draw the approximate crest lines of the contours of  $\beta_i$  for  $n = 1, 2$  on the  $(d, \lambda)$  plane, as illustrated in Fig. 6(b). For

$$n = 1, \quad \theta_2 = 0.3 \sim 0.7, \quad \lambda = 0 \sim 0.5,$$

we find

$$d_{peak} = 1.30 \sim 1.57$$

according to (34). That is why the resonance depth  $d_{peak}$  is always around 1.5 in Figs. 3 and 4.

#### 4 Conclusions

A fractional-order Maxwell model is used to describe the viscoelastic seabed mud. The experimental data of the real mud<sup>[4]</sup> well fit the results of the fractional-order Maxwell model that has fewer parameters than the traditional model. The model is then used to investigate the effect of the mud on the surface-wave damping. The damping rate of a linear monochromatic wave is obtained. The elastic resonance of the mud layer is observed, which leads to the peaks in the damping rate. Near the resonance, the viscosity weakens the mud motion and hence weakens the wave damping. Far from the resonance, the higher viscosity leads to the stronger wave damping. At the resonance point, the larger parameter  $\lambda$  corresponds to the smaller mud depth  $d$ .

The damping rate is a sum of the modal damping rates, which indicates the wave damping induced by the mud motion of particular modes. The analysis shows that near the resonance, the total damping rate is dominated by the damping rate of the corresponding mode. This can be used to find the approximate crest lines of the total damping rate and determine the resonance point on the parameter plane.

#### References

- [1] Sheremet, A. and Stone, G. Observations of nearshore wave dissipation over muddy sea beds. *Journal of Geophysical Research*, **108**(C11), 3357 (2003) DOI 10.1029/2003JC001885

- [2] Jain, M. and Mehta, A. J. Role of basic rheological models in determination of wave attenuation over muddy seabeds. *Continental Shelf Research*, **29**(3), 642–651 (2009)
- [3] Krotov, M. *Water Waves Over a Muddy Seabed*, M. Sc. dissertation, Massachusetts Institute of Technology, 19–35 (2008)
- [4] Jiang, F. and Mehta, A. J. Mudbanks of the southwest coast of India IV: mud viscoelastic properties. *Journal of Coastal Research*, **11**(3), 918–926 (1995)
- [5] Hilfer, R. *Applications of Fractional Calculus in Physics*, World Scientific Publishing, River Edge, New Jersey (2000)
- [6] Xia, Y. Z. and Zhu, K. Q. A study of wave attenuation over a Maxwell model of a muddy bottom. *Wave Motion*, **47**(8), 601–615 (2010)
- [7] Liu, P. L. F. and Chan, I. C. On long-wave propagation over a fluid-mud seabed. *Journal of Fluid Mechanics*, **579**, 467–480 (2007)